

Relaxation oscillations of low-frequency Ar/SF₆ inductive plasma discharges

M Tuszewski, R R White and G A Wurden

Los Alamos National Laboratory, Los Alamos, NM 87545, USA

E-mail: mgtu@lanl.gov


Received 17 December 2002, in final form 19 April 2003

Published 3 June 2003

Online at stacks.iop.org/PSST/12/396

Abstract

A new class of relaxation oscillations has been observed in some inductive plasma discharges operated with low-pressure argon and SF₆ gas mixtures. Some plasma instability seems to develop periodically in the downstream plasma. The nonlinear evolution and the two-dimensional spatial structure of the instabilities are detailed with Langmuir probe arrays and fast video imaging. The measurements show that the instabilities grow in a quasi-spherical downstream layer. The upstream plasma is slightly compressed, while large rarefactions are observed downstream. The upstream plasma then moves slowly downward until the initial plasma profiles are recovered.

 This article features multimedia enhancements

1. Introduction

Inductively coupled plasmas (ICPs) operated with low (1–100 mTorr) gas pressures are often used for materials processing [1]. Many industrial ICPs use electronegative gas mixtures. Stable discharges, where most parameters can be controlled, are often required for such processes. However, relaxation oscillations are sometimes observed in ICP discharges operated with electronegative gases [2–5]. The oscillations perturb significantly the discharges. Hence, understanding their causes and developing control strategies is of practical interest.

Density oscillations were first noticed with Langmuir probes in the downstream region of a 0.46 MHz ICP [2]. Oscillations occurred for some discharges operated with oxygen and with mixtures of argon and SF₆ (Ar/SF₆) gases. Argon or nitrogen discharges were always stable. The ICP source plasma was not explored, and the cause of the oscillations was not established.

Relaxation oscillations were later observed in planar ICP discharges [3, 4]. For a given Ar/SF₆ gas pressure, global source oscillations occurred in a narrow range of the 13.56 MHz radio frequency (rf) power. Stable capacitive and inductive discharges were obtained for lower and higher rf powers, respectively. Zero-dimensional models clearly showed that the capacitive to inductive transitions of

electronegative discharges could be unstable, causing source oscillations consistent with the data.

More recently, the relaxation oscillations of Ar/SF₆ discharges generated in a new 0.46 MHz ICP have been studied [5] in order to clarify the original oscillations [2]. The new data suggest periodic instability growth at some downstream location, hence the name downstream instabilities. One-dimensional, linear, fluid, and kinetic calculations indicate that ion two-stream instabilities might well explain the data.

The nonlinear evolution and the two-dimensional spatial structure of the downstream instabilities are detailed in this paper with Langmuir probe arrays and with a fast video camera. Supporting data from a microwave interferometer and from a visible light monitor are also included. This study does not include a new theoretical analysis. However, the data can be used to benchmark linear instability calculations and possible future numerical simulations.

The ICP plasma source and the diagnostics are described in section 2. The instability domain is presented in section 3. The axial distribution of the oscillations, from probes on axis, is detailed in section 4. The two-dimensional spatial structure of the oscillations is studied in section 5 with fast video imaging and radial probe arrays. The data are discussed in section 6 and some concluding remarks are offered in section 7.

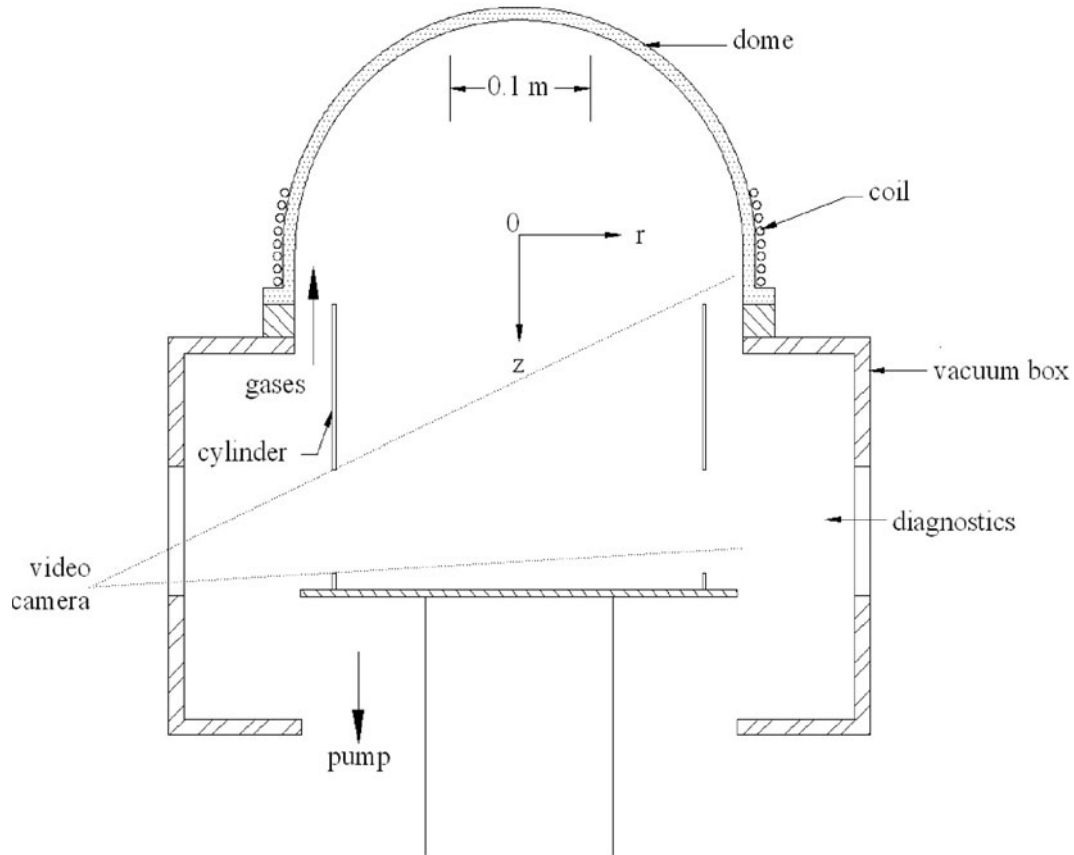


Figure 1. Sketch of the experiment.

2. Experimental apparatus

The 0.46 MHz hemispherical ICP is sketched in figure 1. It consists of an 8-turn coil wound around a quartz dome of 0.36 m inner diameter. The coil mid-plane ($z = 0$) coincides with the centre of the spherical dome. The values of z are measured downward from the coil mid-plane. The coil is powered with continuous 0.46 MHz rf from a 1 kW power supply, via a matching network. Typical reflected powers are 5–10 W. The net rf powers quoted in this paper are forward minus reflected generator powers.

The plasma flows down into a stainless steel cylinder of 0.3 m diameter and 0.22 m length. Premixed argon and SF₆ gases are introduced near the bottom of the quartz dome. The SF₆ fractional concentration is defined as the ratio of the SF₆ partial pressure to the total gas pressure. Typical flow rates are 10–100 sccm, and the gas residence times are about 1 s. The apparatus and the main discharge parameters are detailed elsewhere [6].

Plasma diagnostics are introduced through access ports at $z = 0.24$ m. Cylindrical Langmuir probes with nickel tips (diameter: 0.5 mm, length: 5 mm) are arranged in axial or radial arrays. A planar probe is also used [6]. The probes are operated with a fixed electrical bias of -50 V and with chokes tuned at the rf frequency and its first harmonic. In addition, current–voltage characteristics (-50 to $+30$ V) are acquired with a hidden analytical ESP probe.

A 35 GHz microwave interferometer [7] is aligned along a diameter to monitor the line-integrated electron

density. A fibre optics and photomultiplier tube combination (250–650 nm light transmission) is also used next to the interferometer path. A fast video camera (Vision Phantom IV) views the plasma through a large access port, as indicated in figure 1. The data are acquired with a 4-channel, 400 MHz, Gould digital oscilloscope connected to a computer via RS232 cable.

3. The instability domain

Four Ar/SF₆ discharge parameters have been explored experimentally: (a) the total gas pressure, (b) the net rf power, (c) the SF₆ fractional concentration, and (d) the length of the downstream region. The domain of rf power versus total gas pressure where downstream instabilities occur is shown in figure 2, for discharges with a 50% SF₆ fractional concentration, and for the maximum downstream length sketched in figure 1.

For a given gas pressure, unstable discharges are found between a minimum rf power necessary to sustain a discharge and a maximum rf power in the range 0.6–0.75 kW. The minimum rf power level increases with gas pressure. For gas pressures larger than about 25 mTorr, the minimum sustaining power exceeds the maximum power, and only stable inductive discharges are obtained.

The minimum sustaining power presumably arises because the dielectric capacitive impedance greatly exceeds the coil inductive impedance at 0.46 MHz rf frequency.

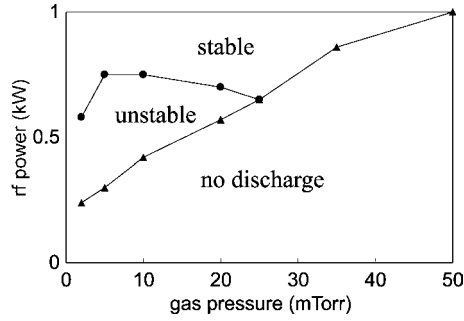


Figure 2. Instability domain of Ar/SF₆ (1 : 1) discharges.

Hence, capacitive currents are negligible and capacitive discharges cannot be sustained for low rf powers. All sustained discharges appear to remain inductive at all times. The reflected rf powers can always be nulled, even in the presence of instabilities.

The downstream instabilities show little variation within the unstable domain of figure 2. The frequencies of the relaxation oscillations increase weakly with gas pressure, from about 0.6–0.7 kHz at 2 mTorr to about 1–1.3 kHz for 5 mTorr and higher gas pressures. The oscillation frequencies vary little with rf power. Similar results are obtained for other SF₆ fractional concentrations. The unstable domain tends to shrink as the SF₆ concentration is reduced. No oscillations are detected for SF₆ fractional concentration less than 25–30%.

The downstream instabilities disappear with sufficiently short downstream plasma lengths. A grounded flat electrode of 0.2 m diameter was placed at various heights inside the downstream cylinder. The instabilities were monitored with probes located on axis above the electrode. Only stable discharges were observed when the electrode was raised to values of z less than 0.14 m. Instabilities occurred for lower electrode heights.

In the next sections, downstream instabilities are detailed for Ar/SF₆ discharges sustained with (a) 2 mTorr total gas pressure, (b) 0.5 kW net rf power, (c) 50% SF₆ fractional concentration, and (d) the maximum downstream length shown in figure 1. Low gas pressures offer somewhat more repeatable oscillations, more details because of reduced collisional damping, and somewhat lower oscillation frequencies. The latter help a video camera imaging limited to 10 frames per millisecond.

4. Axial distribution on axis

A typical oscillation axial structure on axis is shown in figures 3 and 4 for positive ion densities. Dotted and solid lines are alternated in figure 4 to minimize confusion between the various traces. The discharges of figures 3 and 4 are different, but the common probe at $z = 0.18$ m permits a time reference between the top and bottom regions. The time origins are chosen at the beginning of one of the 1.5 ms long oscillation cycles.

The oscillations show the following simplified time sequence: (a) at $t = 0$, a 100 kHz noise appears in the plasma source while densities are approximately steady everywhere, (b) at $t \sim 0.25$ ms, positive and negative density spikes

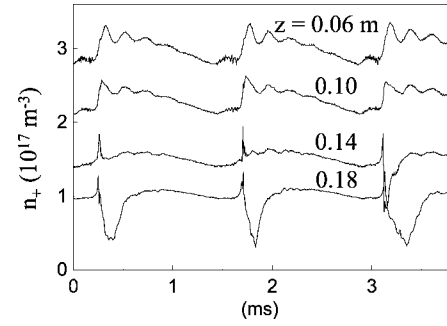


Figure 3. Upstream axial ion density profiles on axis.

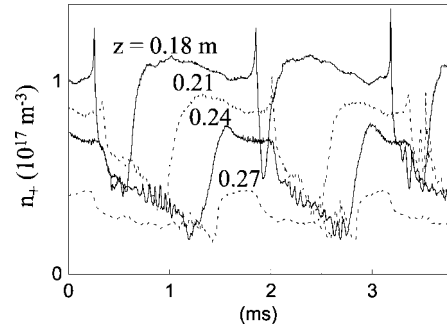


Figure 4. Downstream axial ion density profiles on axis.

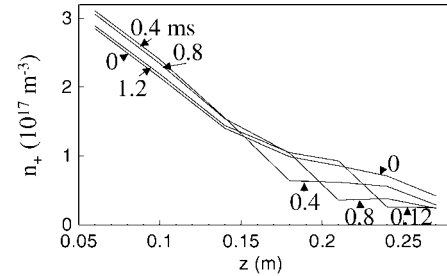


Figure 5. Average axial ion density profiles measured at 0.4 ms intervals during an instability cycle.

develop in tens of microseconds at some critical axial location ($z_c \sim 0.14$ – 0.16 m) as the bottom density starts to drop, (c) between $t \sim 0.25$ and 0.4 ms, the density increases by 10–20% upstream of z_c and decreases by 50–70% downstream of z_c , and (c) between $t \sim 0.4$ and 1.5 ms, the density above z_c progressively decreases while a slow density refilling front propagates below z_c towards the bottom plate.

The average axial ion density profiles, from 10 oscillation cycles, are shown in figure 5 at 0.4 ms time intervals. At $t = 0$, the density decreases nearly exponentially towards the bottom plate. At $t = 0.4$ ms, a two-region profile has formed, including a parabolic-like region upstream of z_c and a relatively flat region downstream of z_c . At $t = 0.8$ and 1.2 ms, the density refilling front moves towards the bottom plate. At $t \sim 1.5$ ms, the initial profile is approximately recovered and a new cycle begins.

The critical location z_c varies by about 10–20 mm from cycle to cycle. For example, z_c is somewhat larger than 0.14 m during the first two oscillation cycles in figure 3, but it is very close to 0.14 m during the third cycle. The critical location z_c tends to increase with total gas pressure. The critical location

z_c also increases with rf power, and approaches the bottom plate near the transition to stable discharges.

The spatial distribution of electron density is also of interest since n_e approximates well visible light emission, as will be shown later in this section. The values of n_+ and n_e can be estimated by combining planar and cylindrical probe data [4–6]. We use a planar probe biased at -50 V and a cylindrical probe biased at a fixed voltage (10–20 V) equal to the plasma potential of a marginally stable discharge. The probes are separated by about 20 mm around $r = 0$ at each z location. Argon discharges are used to infer the effective probe area ratio [6].

The resulting values of n_+ and n_e are shown in figures 6, for z values above, below, and well below z_c . The n_+ data are similar to those of figures 3 and 4, except that the large-size planar probe is somewhat perturbing. The values of n_e vary relatively little. Modest n_e increases occur after the ion density spikes. The ratios n_+/n_e remain in the range 4–5 upstream of z_c , but transiently decrease down to 1 below z_c .

The above two-probe estimate of n_e may be inaccurate during oscillations. However, a separate n_e estimate can be obtained at $z = 0.24$ m with the microwave interferometer. The values of n_+ from a probe and of n_e from the interferometer are shown in figure 7. A 0.3 m long interferometer path and a uniform n_e radial profile are assumed. The average values of n_e are qualitatively similar in figures 6(c) and 7, but the interferometer amplitude variations are somewhat larger.

The light of a fibre optics collimated along a diameter next to the interferometer path length is also shown with dotted lines in figure 7. The photomultiplier tube output level is

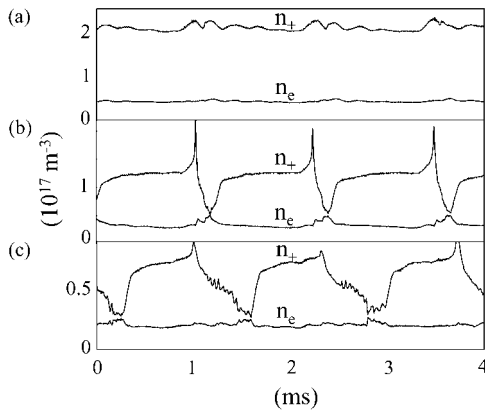


Figure 6. Probe ion and electron densities at $z = (a)$ 0.12, (b) 0.18, and (c) 0.24 m.

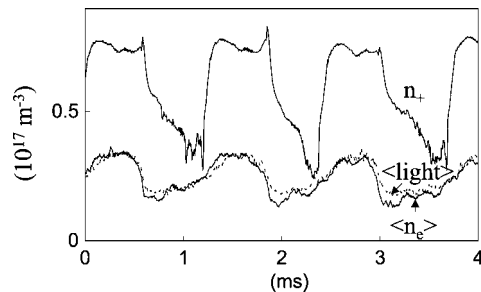


Figure 7. Probe and interferometer densities at $z = 0.24$ m.

adjusted to match the microwave interferometer trace. The line-integrated light and n_e time variations are quite similar, as expected from electron excitation of neutrals. Hence, the visible light imaging of the next section probably approximates well the n_e integrated spatial variations.

5. Two-dimensional spatial structure

Two fast video camera movies of Ar/SF₆ discharges are included in figure 8. The first movie gives a global view, while the second relates images to probe data. The images are artificially coloured from red (high intensity) to blue (low intensity). The time resolution is about a half-frame duration. Double-clicking on either image starts the movie in the electronic version of this paper. The main features of the movies are illustrated with selected frames in figures 9 and 10, for the benefit of all readers.

In the first movie (figure 8(a)), the camera covers the wide field of view indicated with dotted lines in figure 1. The movie consists of 60 frames of 0.1 ms exposure, covering 4 oscillation cycles. Quasi-spherical purple (medium intensity) regions appear suddenly at frames 1, 16, 30, and 46, and then move slowly (~ 0.15 km s⁻¹) downward. Part of the third cycle is shown in figure 9. The downstream region is dim (frame 29) before a purple crescent appears (frame 30). The slow downward motion is seen during the next frames (31–37). A red portion of the plasma source is seen in all but the first frame. Its lower boundary corresponds to the bottom rim ($z = 0.06$ m) of the quartz dome.

In the second movie (figure 8(b)), the camera focuses on the tip of a cylindrical Langmuir probe. The tip is biased at -50 V and is located on axis at $z_c \sim 0.16$ m. The movie consists of 22 frames of 0.17 ms exposure. These frames are located with numbers and with vertical lines on the probe trace of figure 10. Selected image pairs, above the probe trace, show the sudden appearances of the purple regions (frames 3, 11, and 19) at the times of ion density spikes.

The data in figures 8–10 show that the purple regions are formed *(a)* in approximate coincidence with the probe density spikes, *(b)* in the vicinity of the critical locations z_c rather than

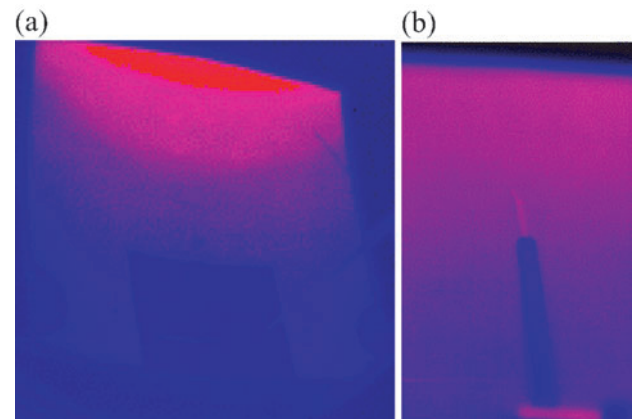


Figure 8. Fast video movies with *(a)* wide and *(b)* narrow field of views.

AVI movies of this figure are available from stacks.iop.org/psst/12/396

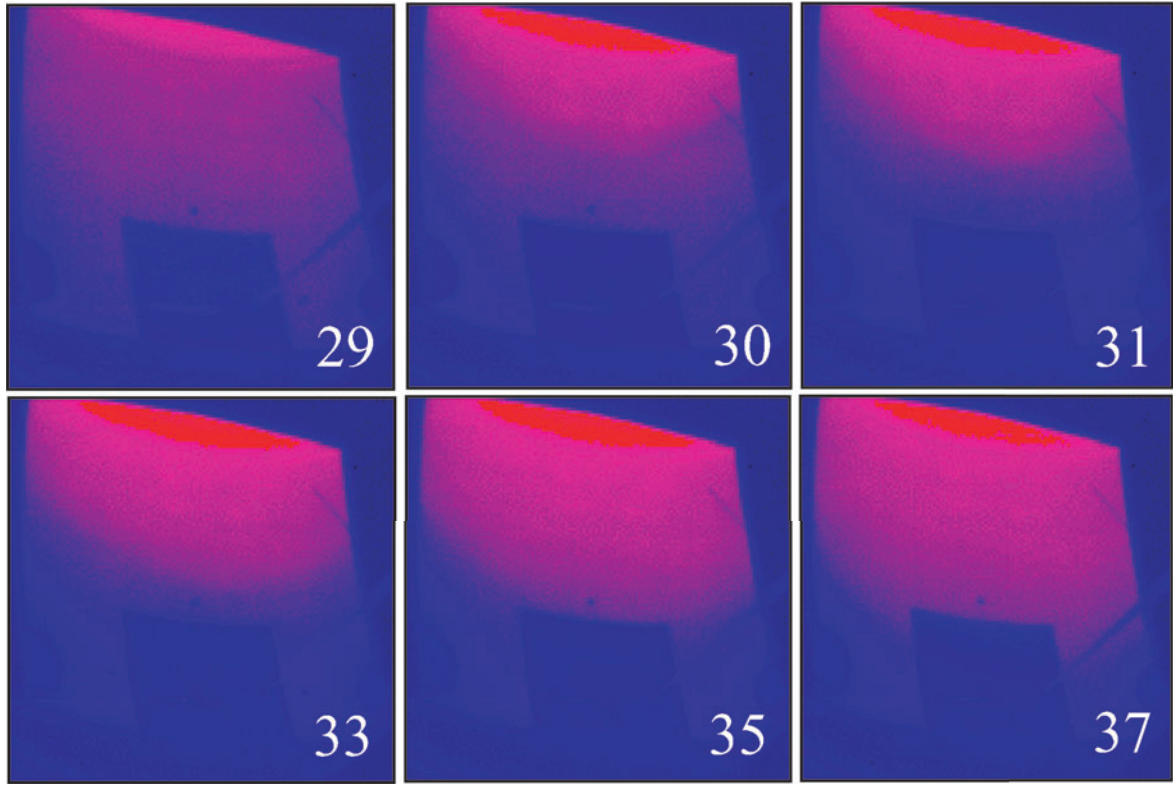


Figure 9. Fast video images of part of an oscillation cycle.

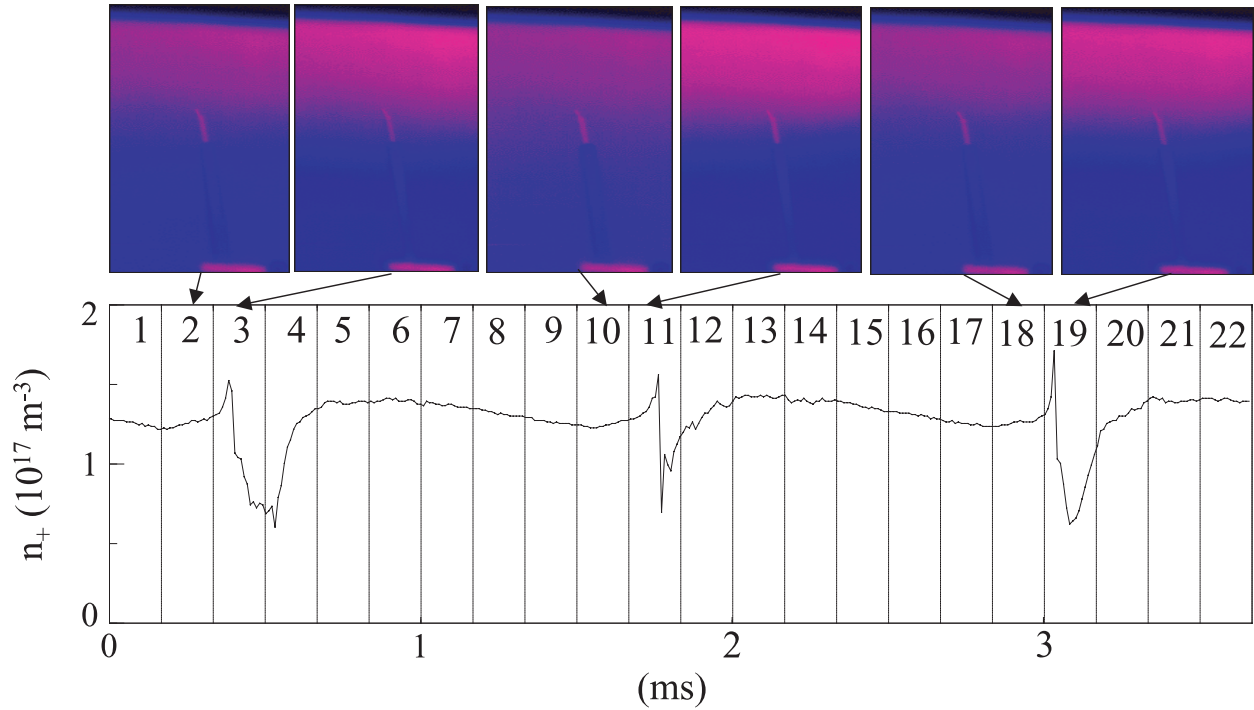


Figure 10. Simultaneous fast video images and probe data.

inside the plasma source, and (c) with quasi-spherical shapes. The images can be related to the probe data on axis of the previous section. The slightly compressed plasmas upstream of z_c correspond to the purple regions. The density refills downstream of z_c correspond to the slow downward motions.

The spherical shape of the critical layer can also be inferred with a radial array of Langmuir probes at $z = 0.16 \text{ m}$, as shown in figure 11. The density refills of probes located at larger radii occur increasingly later relative to the density spikes. These time lags are consistent with a spherical plasma volume

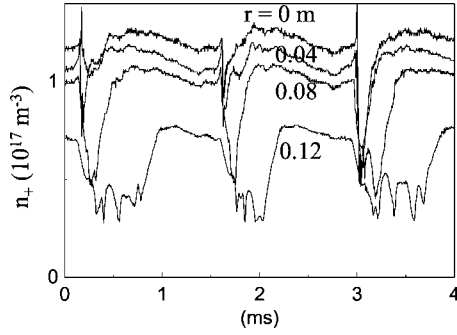


Figure 11. Ion density radial profiles at $z = 0.16$ m.

of 0.15 m radius moving downstream with an axial speed of 0.15 km s^{-1} .

The spherical shape of the refill plasma may also explain in part larger n_e amplitudes in figure 7 than in figure 6(c). The interferometer path length increases during the spherical-like density refill. However, a fixed path length was assumed at all times in calculating n_e in figure 7. Assuming a varying path-length consistent with the spherical shape would yield smaller n_e amplitudes in figure 7.

The spherical shape of the purple regions is best observed when the video camera looks horizontally into the downstream cylinder. Quasi-spherical light fronts were clearly observed, with good symmetry about the z -axis. Movies taken with the video camera looking vertically into the dome through a 45° mirror did not show any appreciable time-dependent features, presumably because the light intensity is dominated by the quiescent plasma source volume.

6. Discussion

Probes on axis indicate that ion density perturbations grow, on microsecond timescales, at a particular downstream location named the critical layer. The plasma upstream of the layer is somewhat compressed but remains largely undisturbed. Large density variations are observed below the layer, on millisecond timescales, until the initial plasma profiles are recovered.

The ion density data of figures 3 and 4 show several unexplained features, including a 100 kHz noise of about 0.2 ms duration before the density spikes, 5 kHz oscillations during the slow density decreases of the upstream plasma, and 20 kHz oscillations during the slow density decreases of the downstream plasma.

The electron density data of figures 6 and 7 present much smaller variations than the corresponding ion density data. The electron densities merely show modest increases after the ion density spikes. The downstream plasma becomes transiently electropositive, which may indicate internal sheath formation [8–10]. Visible light emission approximates well the integrated electron densities.

The video camera images show that the critical layers, where the density spikes form periodically, are quasi-spherical in shape. This is consistent with data from radial probe arrays in the downstream region. The video camera is not fast enough to capture the detailed formation of the density spikes. However, the subsequent slow density refills are well resolved.

These relaxation oscillations differ substantially from the source oscillations seen in 13.56 MHz planar ICPs [3–4]. The downstream instabilities have (1) lower frequencies by about one order of magnitude, (2) much smaller density variations within the ICP source plasma, and (3) much stronger spatial dependences in the downstream region. Capacitive to inductive transitions presumably cannot occur in this ICP because capacitive Ar/SF₆ discharges cannot be sustained for low rf powers.

Neutral gas dynamics could perhaps explain this oscillations, as was proposed for some other discharges [11, 12]. The oscillation frequencies (~ 1 kHz) are consistent with gas transport timescales. The density refilling speed ($\sim 0.15 \text{ km s}^{-1}$) approximately matches the room temperature Ar/SF₆ gas speed. However, it is difficult to see how neutral gas depletion could lead to local phenomena at a critical layer. Besides, neutral gas effects would occur with all gas chemistries, including pure argon discharges.

A perhaps more promising explanation is that some plasma instability develops periodically at the critical layer. The linear growth of the instability would produce the positive density spikes. The nonlinear phase of the instability would cause the subsequent large density perturbations. The initial density profile would then be slowly recovered and a new instability cycle would begin. Ion two-stream instabilities have been identified as a likely mechanism [5]. Including radial flows in a two-dimensional analysis could yield spherical-like instability layers.

Numerical simulations are required to model the nonlinear evolution of the instabilities. A two-dimensional numerical model may be necessary for a detailed comparison with the data. However, a one-dimensional simulation may capture the dominant axial structure of the oscillations. Electronegative plasma expansion into a vacuum region has been recently studied with a one-dimensional particle-in-cell simulation [13]. Instabilities, consistent with ion two-stream, were observed. The simulations showed a quiescent period before instability onset, small upstream variations, and large downstream perturbations. These features are qualitatively similar to some of the present observations.

7. Conclusions

Relaxation oscillations are observed for some low-pressure Ar/SF₆ discharges sustained in a 0.46 MHz hemispherical ICP. Langmuir probe and fast video camera data reveal the strong spatial structure of the oscillations. Ion density spikes develop periodically in tens of microseconds in a quasi-spherical critical layer well below the plasma source. The upstream plasma is then slightly compressed, while the downstream plasma experiences large rarefactions and subsequent density refills.

The localized growth of density spikes suggest that some instability may develop periodically in the downstream plasma. These observations provide information on the two-dimensional spatial structure and on the nonlinear evolution of the instabilities. Future numerical simulations, benchmarked against the data, would be useful to confirm the nature of the instabilities.

Acknowledgments

This research was conducted under the auspices of the US Department of Energy, through funds provided by the University of California for the conduct of discretionary research by Los Alamos national Laboratory.

References

- [1] Lieberman M A and Lichtenberg A J 1994 *Principles of Plasma Discharges and Materials Processing* (New York: Wiley)
- [2] Tuszewski M 1996 *J. Appl. Phys.* **79** 8967
- [3] Lieberman M A, Lichtenberg A J and Marakhtanov A M 1999 *Appl. Phys. Lett.* **75** 3617
- [4] Chabert P, Lieberman M A, Lichtenberg A J and Marakhtanov A M 2001 *Plasma Sources Sci. Technol.* **10** 478
- [5] Tuszewski M and Gary S 2003 *Phys. Plasmas* **10** 539
- [6] Tuszewski M and White R R 2002 *Plasma Sources Sci. Technol.* **11** 338
- [7] Tuszewski M and Tobin J A 1996 *Plasma Sources Sci. Technol.* **5** 640
- [8] Kouznetsov I G, Lichtenberg A J and Lieberman M A 1999 *J. Appl. Phys.* **86** 4142
- [9] Lichtenberg A J, Lieberman M A, Kouznetsov I G and Chung T H 2000 *Plasma Sources Sci. Technol.* **9** 45
- [10] Franklin R N 2001 *Plasma Sources Sci. Technol.* **10** 162
- [11] Degeling A W, Sheridan T E and Boswell R W 1999 *Phys. Plasmas* **6** 1641, 3664
- [12] Garrigues L, Heron A, Adam J C and Boeuf J P 2000 *Plasma Sources Sci. Technol.* **9** 219
- [13] Medvedev Yu V 2002 *Plasma Phys. Control. Fusion* **44** 1449